J. Phys. B: At. Mol. Opt. Phys. **23** (1990) 959-979. Printed in the UK

A detailed analysis of H($n = 2, 3$) excitation in low-energy H + Ar and H + Xe collisions

J Grosser, W Krüger, W Steen and H Voigt

Institut für Atom- und Molekülphysik, Universität Hannover, Federal Republic of Germany

Received 26 June 1989, in final form 2 October 1989

Abstract. The integral partial cross sections for the processes H + Ar, Xe → H(2s), H(2p), H(3s), H(3p), H(3d) have been measured for collision energies from threshold to 1.5 keV. They were obtained from an analysis of the intensity variation of the emitted light under the influence of a weak electric field, which was applied to the collision region. The method yields in addition a number of $n = 2$ and $n = 3$ off-diagonal density matrix elements (e.g. the sp coherence) and $n = 3$ polarisation data.

1. Introduction

The inelastic collision processes of hydrogen atoms with noble gas atoms have been the subject of constant interest for more than 20 years (see, for instance, Dose *et al* 1968, Orbeli *et al* 1969, Birely and McNeal 1972, VanZyl *et al* 1986). Besides the importance of the data for astrophysical questions, one main reason is the unexpected complexity of these systems. This makes them a good testing field for both our experimental and theoretical abilities in the field of atom-atom collisions. Experimentally, sophisticated methods are required to distinguish the numerous inelastic channels from each other. For H + Ar, for instance (figure 6), the channels leading to H(2s), H(2p), H(3s), H(3p), H(3d), H(4p or 4d), H(4s), $H^+ + Ar + e$, $H + Ar^+ + e$, and $H^- + Ar^+$ have cross sections between 10^{-18} cm^2 and 10^{-16} cm^2 in the range of collision energies from threshold to 1 keV (Fleischmann and Young 1969, VanZyl *et al* 1977, 1980, VanZyl and Gealy 1987, Aberle *et al* 1979, 1980, Grosser and Krüger 1985). It is far from trivial to detect the states H(3s), H(3p) and H(3d) separately, to distinguish the charged channels from each other, or to distinguish the direct collisional excitation to H(2p) from a cascade excitation such as $H + Ar \rightarrow H(3d) \rightarrow H(2p) + h\nu$. In addition, the cross sections for the various channels are not the complete experimental information accessible. Non-diagonal elements of the density matrix for the ensemble of collisionally excited H atoms can be measured (Krotkov and Stone 1980). This requires new and even more complicated experimental methods. Theoretically, one has to deal with the excited states of the diatomic hydrogen-noble-gas-atom systems, which, quite obviously in view of the experimental data, possess a multitude of non-adiabatic couplings. Present-day quantum chemical numerical programs are able to deal with such a situation. However, the reliability of such data, especially of the computed coupling matrix elements, is not really known, and sensitive tests are highly desirable.

We present experimental values for the integral cross sections for H(2s), H(2p), H(3s), H(3p) and H(3d) production in H + Ar and H + Xe collisions for energies from the threshold to 1.5 keV. Some of the non-diagonal elements of the density matrix

0953-4075/90/060959+21$03.50

have been determined as well, and some information about the polarisation of the 3d state was obtained experimentally. The data were extracted from measurements of the H_α and L_α emission from a scattering cell in the presence of a weak electric field. The experimental setup is presented in section 2, the principle of the experimental method is discussed in section 3, the data reduction procedure and the experimental results are described in section 4, and section 5 contains a short qualitative discussion in terms of molecular potentials and non-adiabatic couplings.

2. The apparatus

The hydrogen atoms are produced by laser photodetachment from negative ions (figure 1). This is a well established method, which was described previously (Aberle *et al* 1979, 1980). Typical beam intensities are 4×10^8 atoms/s, and the beam energy is variable down to 10 eV. Lower energies are a problem for the following reason. The beam intensity is measured as the current of the detached electrons. This is a reliable method as long as it is certain that all atoms which are produced in the laser field enter the scattering cell. We observe the atomic beam profile in order to control this question. Our beam profile monitor uses the electron production by H atoms on a surface. Because this process becomes very inefficient at low energy (Fleischmann *et al* 1969), the monitor does not work below 10 eV. It cannot be excluded, therefore, that the measured intensity is too large for these energies. We can produce neutral atoms at energies below 10 eV, but we do not have a reliable method to measure the intensity.

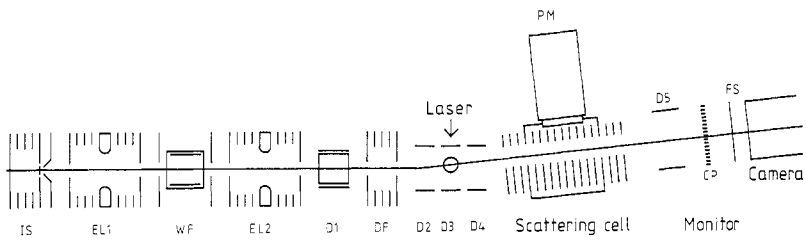

Figure 1. Schematic view of the apparatus: IS, H^- ion source; EL1, EL2, electric lenses; WF, Wien filter for mass selection; D1–D5, deflecting plates; DF, decelerating field; PM, photomultiplier; CP, channel plate; FS, fluorescent screen.

The beam passes through a scattering cell, which is normally operated at a target gas pressure of 5×10^{-4} mbar. This is sufficient to guarantee single collision conditions. Great care was taken to establish a simple, well known gas density distribution in the cell. By a computer simulation it was found that the density is practically constant inside the cell and drops rather suddenly at the entrance and exit holes to the background value, typically 10^{-5} mbar. An electric field, which is parallel or antiparallel to the atomic beam, can be applied to the target region. Care was taken to make the field homogeneous over the entire extension of the gas target. The central part of the cell is viewed by a L_α(122 nm) or a H_α(656 nm) photon detector. The L_α detector is a CuBe open multiplier. The combination of the multiplier with the MgF_2 window of the cell acts as a broad-band L_α filter. In the case of H+Ar, only the photons from

the transitions H(2s, 2p)→H(1s) are detected by this system; for H+Xe, additional contributions from the Xe transitions $5p^5 5d$, 6s, $7s \rightarrow 5p^6$ are possible, which have wavelengths close to the L_α line. The H_α detector is a combination of a broad-band interference filter, small and large wavelength cutoff filters and a photomultiplier. The filter combination has a width of 80 nm FWHM. Once more, for H+Ar this is small enough to exclude all lines which can be expected to occur, except the transitions $H(n=3) \rightarrow H(n=2)$. For H+Xe, a number of Xe transitions, like $5p^5 8p \rightarrow 5p^5 6s$, are within the transmission region. (The H_α filter is designed to have a large angle of acceptance, this requires a broad-band filter.) Typical experimental results are shown in figure 2.

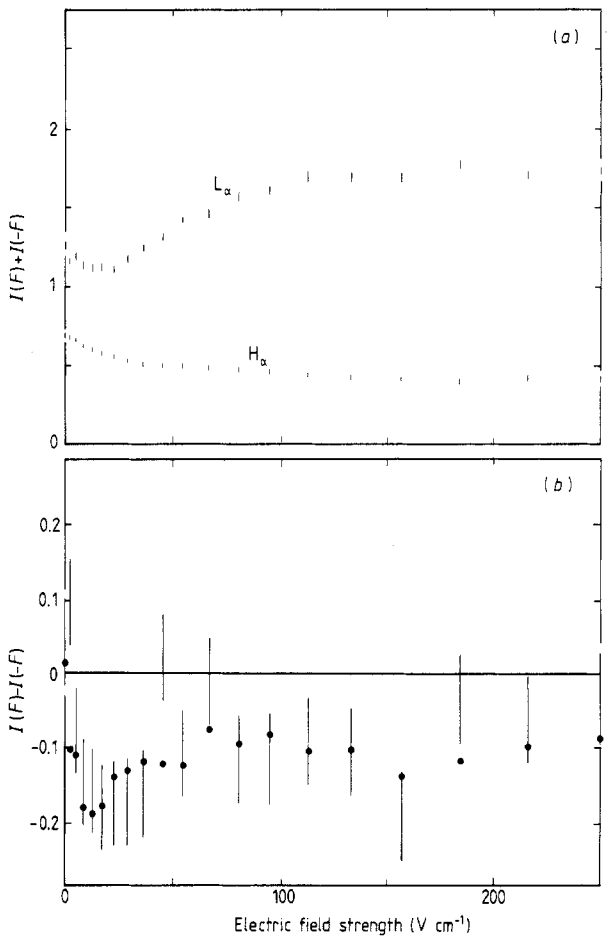

Figure 2. Typical experimental results for the variation of the light intensity I with the strength of the electric field. F and $-F$ stand for an electric field parallel and antiparallel to the direction of the incident beam. (*a*) $I(F)+I(-F)$ in arbitrary units for the L_α and H_α intensities for H+Ar at 350 eV collision energy. The bars show twice the statistical uncertainty. (*b*) The asymmetry $I(F)-I(-F)$ in arbitrary units for L_α (large error bars) and for H_α (circles) for H+Ar at 100 eV. The uncertainty of the H_α values for $I(F)-I(-F)$ is not shown, it is typically one third of that of the L_α values. For both figures, the H_α and L_α data have already the correct relative scaling. The differences $I(F)-I(-F)$ are typically below 10% of $I(F)+I(-F)$.

3. Theory of the experimental method

Quite different methods have been used to detect the l-degenerate states of excited H atoms separately. VanZyl *et al* (1980, 1986) distinguished H(3s) from H(3d) and H(3p) by making use of the longer lifetime of the former. Knize *et al* (1984) applied a microwave resonance optical detection technique to determine, for the processes $H^+ + N_2$, $H_2 \rightarrow H(nlm)$, all partial cross sections $\sigma(3lm)$. The application of a weak electric field was originally proposed and applied to detect the metastable state H(2s). There are numerous experiments, in which H(2s) production cross sections were evaluated from the difference in the L_α intensities, measured with and without an electric field. When higher excited states are present, this simple form of the method fails. The L_α intensity in figure 2(a), for example, has three major components, from the transitions $2p \rightarrow 1s$, $2s \rightarrow 1s$, and $3d \rightarrow 2p \rightarrow 1s$. The intensity of the first component is practically independent of the field strength, the intensity of the second one increases and that of the third one decreases with increasing strength of the field. A more refined method of analysis is obviously needed.

The intensity variations result from the fact that electronic states of the hydrogen atom with different decay properties (lifetimes and branching ratios) are nearly degenerate. A weak electric field is sufficient to mix these states very effectively, thereby changing the decay properties. The collision is a very fast process, its typical time duration is below 10^{-13} s, the subsequent decay process is much slower, of duration 10^{-9} s or more. When the decay is discussed, the collision can be regarded as an instantaneous process, which merely defines the starting conditions for the decay.

A number of small interactions can be neglected when the collision is described. These are

(i) the interaction with the electric field as long as its strength does not exceed some 100 V cm^{-1};

(ii) the interaction with the photon field, that is, the optical decay and the Lamb shift;

(iii) the spin-orbit interaction;

(iv) the hyperfine interactions.

The reason is, that for all these interactions the product $\Delta H \Delta t$ (the magnitude of the interaction multiplied by the time duration of the collision) is small. The statement is easily verified by the time-dependent Schrödinger equation. The result of a collision process in which a hydrogen atom is excited, can therefore be specified by a set of scattering amplitudes $f_{nlm}(\theta)$, which depend upon the principal and orbital angular momentum quantum numbers for the excited state, but not upon the electronic and nuclear spin, and not upon the strength of the external electric field. θ is the scattering angle, and the projection quantum number m is specified with respect to the primary beam direction as the quantisation axis.

Immediately after a collision process, the wavefunction of the excited hydrogen atom has the form $\Sigma_{lm} f_{nlm}(\theta)|nlm, m_s, m_i\rangle$, with m_s and m_i the electronic and nuclear spin-projection quantum numbers; it is sufficient to consider only the states associated with one fixed value of the principal quantum number at a time. The subsequent time evolution of the wavefunction can be determined by solving the time-dependent Schrödinger equation. Practically, one determines the eigenstates of the Hamiltonian and expands the wavefunction with respect to these states. Every eigenstate has its own characteristic frequency and decay time, and the procedure gives immediately the desired time dependence. As the time duration Δt of the optical decay is much larger

than that of the collision, $\Delta H \Delta t$ is no longer small for the small quantities discussed above. For the correct description of the optical decay, these interactions have to be included in the Hamiltonian.

There exists a more principal problem in the quantum mechanical procedure. The usual way to treat the problem of a decaying atom in the external field is as follows. First, one calculates the eigenenergies (characteristic frequencies) in the field, neglecting the decay, and second, one calculates the transition probabilities and decay time constants from the well known matrix element expressions. The procedure is wrong, and it leads to results, which disagree with the correct results, sometimes substantially. The reason is that the decay width of the excited levels is of the same order of magnitude as the other small interactions. This situation requires a fully quantum mechanical treatment of the problem, including the photons. Fortunately, this can be shown (Grisaru *et al* 1973) to be equivalent to a formulation, in which the decay is represented by a decay matrix $i\Gamma$, which has to be added to the particle Hamiltonian. The form of the decay matrix is far from trivial. Our quantum mechanical calculations are therefore based on a complex Hamiltonian, $H + i\Gamma$. H includes the small interactions discussed above except the decay, and $i\Gamma$ is used in the form given by Grisaru *et al* and represents the decay. The eigenstates mentioned above are the eigenstates of this Hamiltonian.

The light intensities $I(t)$ for all possible transitions can be expressed as bilinear forms in the time-dependent wavefunction, leading to expressions of the type

$$I(t) = \sum f_{nlm} f^*_{nl'm'} U_{nlm,nl'm'}(t, m_s, m_i). \tag{1}$$

$I(t)$ as well as the factors U depend upon the indicated quantum numbers, the time t elapsed since the excitation process, the type of radiation considered (e.g. H_α or L_α), the direction of observation and upon the strength and direction of the external field. We calculate the functions U numerically.

In the actual experiment, the time and direction of the observation and the quantum numbers m_s and m_i are not, or not completely, specified, requiring the following averaging or integration procedures.

(i) The intensity is averaged over the electronic and nuclear spin directions. The electronic and nuclear spins are not influenced by the collision (once more, because $\Delta H \Delta t$ is small). The quantum numbers are therefore statistically distributed.

(ii) The intensity is integrated over all those times, which the excited atom spends in the viewing field of the detector. It depends upon the starting point of the excited atom in the scattering cell and upon its direction and velocity, which time interval this is. Direction and velocity are taken to be those of the incident beam, the distribution of the starting points is given by the target gas density distribution in the cell. The procedure covers, for instance, the intensity from atoms, which are produced outside and decay in the viewing field of the photon detector.

(iii) The intensity is integrated over the angular extension of the photon detector.

These integration and averaging procedures affect only the factors $U_{nlmn'l'm'}$ in equation (1). They are carried out numerically as well. The scattering angle of the particles, which is not fixed by the experiment, must be integrated over as well, this replaces the products $f_{nlm} f^*_{nl'm'}$ in equation (1) by integrals over these products. The final result for the light intensity reads, here for L_α light,

$$I(L_\alpha, F) = N \operatorname{Re} \sum_{\substack{n \geqslant 2 \\ l' \geqslant l}} u_{nlm,nl'm}(L_\alpha, F) \sigma_{nlm,nl'm}. \tag{2}$$

A similar expression is valid for the H_α intensity, the sum extends then over all $n \geqslant 3$. I is the experimental photon counting rate, F is the field strength and N is a normalisation factor. A convenient choice is $N = n_1 n_2 \tau v \Delta\omega / 4\pi$, with $n_{1,2}$ the target and projectile number densities, τ the scattering volume, v the relative velocity and $\Delta\omega$ the angular extension of the photon detector. The value of N is without importance for what follows, however. The weighting functions $u(L_\alpha, F)$ and $u(H_\alpha, F)$ are the result of the numerical procedure and the σ are related to the scattering amplitudes,

$$\sigma_{nlm,nl'm} = \int f_{nlm}(\theta) f^*_{nl'm}(\theta)\, \mathrm{d}\Omega. \tag{3}$$

The diagonal terms are the ordinary partial cross sections (we write σ_{nlm} in place of $\sigma_{nlm,nlm}$ in the following, and similarly for the u factors), the non-diagonal terms are density matrix elements, however, with the dimension of a cross section. The term $\sigma_{2s0,2p0}$ is known as the 'sp coherence' term. The cross sections and the diagonal weighting factors are real, the off-diagonal terms possess real and imaginary parts. The sign of the off-diagonal terms depends upon the phase convention used for the wavefunctions $|nlm\rangle$. We used the Condon–Shortley conventions, where the positive z direction coincides with the direction of the incident beam.

With $F > 0$ designating a field parallel and $F < 0$ antiparallel to the incident beam, the weighting factors obey

$$u_{nlm,nl'm}(-F) = (-1)^{l-l'} u_{nlm,nl'm}(F) \tag{4}$$

It is therefore convenient to measure the quantities

$$I(F) + I(-F) = 2N\ \mathrm{Re} \sum u_{nlm,nl'm}(F) \sigma_{nlm,nl'm} \tag{5}$$

with the sum going over $l' - l = 0, 2, \ldots$ and

$$I(F) - I(-F) = 2N\ \mathrm{Re} \sum u_{nlm,nl'm}(F) \sigma_{nlm,nl'm} \tag{6}$$

with the sum going over $l' - l = 1, 3, \ldots$. We will consider in the first instance the values 2 and 3 of the principal quantum number. Then the symmetric combination contains a single off-diagonal term, $\sigma_{3s0,3d0}$, but all cross sections, the antisymmetric combination contains only off-diagonal terms. Figure 3 shows various calculated functions $u(F)$. The functions depend to some extent on the collision energy. With the above choice of the normalisation factor N, the value $u = 1$ corresponds to the following situation: the excited state decays by 100% by emission of the wavelength in question, the decay is so fast that the distance which the excited atoms travel between the excitation and the decay is negligible and the angular distribution is spherically symmetric.

For a reliable calculation of the weighting curves $u(F)$, one must indeed apply the full numerical procedure described above. This does not prohibit qualitative explanations for the shape of some of the curves in figure 3. The H_α and L_α intensities from the 3s and 3d states diminish in the field, because the increasing 3p admixture allows the direct transition to the ground state by emission of a L_β photon, which is not detected. The intensities from the 3p states increase, because the decay path $3p \rightarrow 2p \rightarrow 1s$ opens, but a large fraction remains decaying directly, $3p \rightarrow 1s$. The intensity from the state 2s increases, because the increasing 2p admixture reduces the lifetime by many orders of magnitude, and more and more atoms decay in the viewing field of the detector. The 2p intensity is practically constant, because the lifetime is very short, the two substates have different weight, because the angular distributions are different.

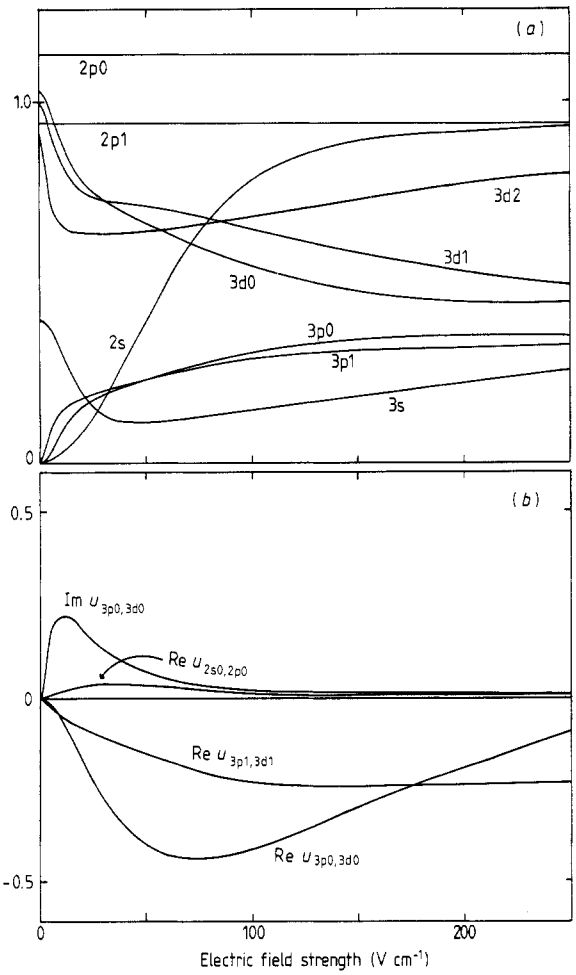

Figure 3. Computed weighting factors for the L_α-intensity. (*a*) Cross section terms appearing in $I(F)+I(-F)$; (*b*) coherence terms appearing in $I(F)-I(-F)$.

Simplified arguments can also be given to explain the form of the non-diagonal weighting factors, but the arguments remain rather complicated, even then. The factors $u(F)$ for the $n=4$ states were not calculated, but they are needed for a discussion of the higher cascade contributions to the signal. The following qualitative description of the diagonal terms was deduced by arguments like those above, using in addition numerical results upon branching ratios for very small field strength (VanZyl *et al* 1988).

The $u_{n=4}(H_\alpha, F)$ are small, except the $u_{4f}(H_\alpha, F)$. The $u_{4f}(H_\alpha, F)$ and the $u_{4f}(L_\alpha, F)$ are similar to the u_{3d} curves in figure 3, with an even more rapid variation near zero field strength (the increasing 4d admixture causes 4f → 3p → 1s and 4f → 2p → 1s transitions). $u_{4d}(L_\alpha, F)$ begins with a value 0.75 at zero field and decreases similar to u_{3d} when the field increases (4p admixture causing 4d → 1s decay). $u_{4p}(L_\alpha, F)$ is similar to u_{3p} (increasing 4s and 4d admixture) and $u_{4s}(L_\alpha, F)$ decreases from 0.6 to slightly smaller values (4p admixture causing 4s → 1s decay).

In order to check the reliability of the computed weighting factors, we compared $n=3$ branching ratios computed with our program with data obtained by Rouze *et al*

(1986). Branching ratios do not depend on geometrical data. We found a complete agreement. Errors can be thought to occur in the integration procedures, but the geometrical data of the cell and the gas density distribution are well known. When calculating the time period, which an excited atom spends in the viewing field of the detector, we neglect the deviation of the scattered atom from the direction of the incident beam. This is sufficiently well justified at high collision energy, and it is uncritical for low collision energy, because then the atoms travel only short distances before decaying. The quantum mechanical calculation is performed with a constant electric field. This is correct, because the field is homogeneous over the entire distribution of the target gas and of the viewing field. We conclude that the computed factors $u(F)$ are practically correct.

4. Data reduction and results

4.1. Cross sections

The cross sections are evaluated from the experimental data $I(F)+I(-F)$ for the L_α and the H_α intensities, as in figure 2(*a*). The evaluation procedure consists in fitting the experimental data by linear combinations of the weighting curves $u(F)$, with the σ as the unknown fitting parameters. In order to reduce the number of fitting parameters, the following approximations and neglections are made:

(i) the curves u_{3p0} and u_{3p1}, which are very similar, are replaced by their mean value;
(ii) the term with $\sigma_{3s0,3d0}$ is neglected;
(iii) all contributions with $n>3$ are neglected.

The quantities which remain to be determined are the cross sections σ_{2s}, σ_{2p}, σ_{3s}, $\sigma_{3p}=\sigma_{3p0}+\sigma_{3p1}$, σ_{3d0}, σ_{3d1} and σ_{3d2}. The sublevels of the state 2p cannot be resolved by the fit, the calculations were performed with $u_{2p}=1$. This means that we determine the quantity $1.13\sigma_{2p0}+0.94\sigma_{2p1}$. For simplicity, this is denoted as σ_{2p} in the following. It turned out that a fit to the L_α data alone is not sufficient to obtain the cross sections with a reasonably small error. For this reason, the H_α data were measured in addition. In order to allow a comparison of the L_α and H_α data sets, the relative sensitivity of the L_α and H_α detection systems must be known. We proceed as follows. In the first step, the H_α data are evaluated, giving values for the five $n=3$ cross sections. With these values, the cascade contribution to the L_α signal is calculated. Next the experimental L_α data are fitted by a linear combination of the cascade data with the curves $u_{2s}(F)$ and $u_{2p}(F)$. The procedure gives the factor, by which the calculated cascade data have to be multiplied for the best fit. Because the calculated cascade data are in the units of the H_α results, this factor contains the relative calibration of the two data sets. The procedure was repeated for different collision energies, and the ultimate value for the calibration factor was obtained as an average. In the last step, the subtraction of the cascade data from the L_α data and the evaluation of σ_{2s} and σ_{2p} was repeated, using the ultimate value for the calibration factor. In a few cases, interpolated H_α data were used for the cascade correction.

We obtain in this way the $n=2$ and $n=3$ cross section values with the correct relative scaling for each of the two collision systems. The relative scaling of the Ar and Xe data and the absolute cross section scale is not obtained from our experiment. We scaled our data in accordance with the L_α emission cross section data published by VanZyl and Gealy (1987), which have an error margin of ±15% for the absolute cross section scale, the polarisation correction was duely taken into account. The final

results for the cross sections σ_{2s}, σ_{2p}, σ_{3s}, σ_{3p} and $\sigma_{3d} = \sigma_{3d0} + \sigma_{3d1} + \sigma_{3d2}$ are given in the tables 1 and 2. The indicated error represents the statistical uncertainty. It is obtained from the covariance matrix, which is generated from the statistical error of the original data by the fitting procedure (Bevington 1969). The fit yields separate values for the partial cross sections σ_{3dm} for $m = 0, 1, 2$. These values normally have rather large uncertainties. The three values are highly correlated (large off-diagonal elements of the covariance matrix), however, reflecting the fact that the three weighting curves $u_{3dm}(F)$ are quite similar. The statistical error of the sum σ_{3d} is therefore significantly smaller than the typical uncertainty of the σ_{3dm}. Figures 4 and 5 show σ_{3d0}/σ_{3d} and σ_{3d1}/σ_{3d} as obtained from the fit. The statistical error of σ_{2p} and σ_{2s} in the tables includes a contribution from the uncertainty of the H_α-L_α calibration factor (±10%). The indicated uncertainties do not include the uncertainty of the absolute scaling. Our absolute scales are uncertain to ±15%. The relative scaling of the $n = 2$ and the $n = 3$ data is uncertain to ±10%, this is the uncertainty of the calibration factor.

Systematic errors can arise in our data from the simplifications described above. The replacement of u_{3p0} and u_{3p1} by single curves has practically no influence upon the final results, as witnessed by a numerical simulation. The weighting factor $u_{3s0,3d0}$ is small and the corresponding σ term cannot be large (because $\sigma_{3s0,3d0} \leqslant \sqrt{\sigma_{3s0}\sigma_{3d0}}$). The influence upon the final results is negligible. Cascades from $n = 4$ states can have the following effects.

4f. Our method practically does not distinguish between a 3d and a 4f excitation. If there is a 4f excitation, we expect the cross section to be contained essentially in the evaluated 3d cross section. It cannot be excluded with certainty, however, that for instance the additional maximum in σ_{3s} for Ar at low energy is partly an artefact caused by 4f cascades. The question remains open as long as the 4f production cross section and the exact behaviour of u_{4f} are unknown.

4d and 4p. The 4d cross sections are practically known, the 4p cross section is practically unknown (VanZyl *et al* 1980, 1986). Their cascade contributions can result in an error of up to 10% in the determination of the L_α-H_α calibration factor and hence in the absolute scaling of the $n = 3$ cross sections. Further, the evaluated 2p cross section might be somewhat overestimated by this effect. However, when σ_{4p} does not exceed σ_{4d}, this error is only of the order of a few per cent for most of the data points; the largest correction which is expected in such a case occurs at the minimum of σ_{2p} for Ar at 200 eV and might reduce the cross section value by as much as 15%.

4s. The cross sections are known. They are so small that cascade effects are negligible.

Cascades from higher states are expected to be negligible, when the cross sections are below the known $n = 4$ cross sections. In the case of H+Xe, additional complications arise, when radiation from excited Xe atoms contributes to the observed signals. The corresponding intensities do not depend upon the electric field strength. A contribution to the L_α intensity would therefore enlarge our value for σ_{2p}. The good agreement of our L_α emission cross section data with the corresponding result of VanZyl and Gealy (1987) implies that the Xe emission in the L_α wavelength region is much smaller than the L_α emission. A Xe contribution to the measured H_α intensity would result primarily in a wrong determination of the H_α-L_α calibration factor. Indeed, there is a slight difference between the calibration factors evaluated from the Ar and the Xe experiments, which might indicate that the corresponding Xe excitation cross sections are as large as 30% of σ_{3d} for H+Xe. Such a contribution would not affect the evaluated 2s, 2p, and 3s cross sections. The 3d cross section would be smaller

Table 1.

H atom kinetic energy	$H(1s)+Ar \rightarrow H(nl)$ integral cross sections (10^{-17} cm^2)				
	σ_{2s}	σ_{2p}	σ_{3s}	σ_{3p}	σ_{3d}
12.3	0.52 ± 0.09	0.81 ± 0.10			
13.0	0.76 ± 0.13	1.35 ± 0.13			
13.5	0.99 ± 0.09	1.31 ± 0.08			
13.8	1.39 ± 0.10	0.99 ± 0.06			
14.1	1.78 ± 0.12	0.82 ± 0.06			
15.0	2.53 ± 0.15	0.54 ± 0.05			
15.5	2.48 ± 0.10	0.66 ± 0.04			
16.0	2.74 ± 0.17	0.65 ± 0.06			
16.5	2.37 ± 0.10	1.25 ± 0.06			
17.0	1.95 ± 0.09	1.95 ± 0.08			
18.0	1.78 ± 0.14	2.26 ± 0.13			
18.5	1.21 ± 0.10	3.22 ± 0.12			
19.0	0.85 ± 0.10	3.71 ± 0.14			
19.5	0.72 ± 0.07	3.74 ± 0.13			
20.0	0.66 ± 0.19	3.31 ± 0.13	−0.01 ± 0.19	0.09 ± 0.40	0.25 ± 0.27
21.5	0.69 ± 0.24	3.70 ± 0.17			
22.0	0.80 ± 0.23	4.02 ± 0.16			
23.0	0.73 ± 0.21	4.37 ± 0.15			
24.0	1.02 ± 0.21	4.41 ± 0.14			
25.0	1.39 ± 0.18	4.40 ± 0.12	0.16 ± 0.09	0.44 ± 0.18	0.54 ± 0.13
28.0	2.17 ± 0.19	3.80 ± 0.12			
30.0	3.73 ± 0.31	3.63 ± 0.19	0.34 ± 0.13	0.90 ± 0.26	1.09 ± 0.18
35.0	5.95 ± 0.36	3.46 ± 0.21	0.28 ± 0.15	0.62 ± 0.28	1.97 ± 0.20
37.0	6.80 ± 0.39	3.36 ± 0.23			
40.0			0.25 ± 0.13	0.74 ± 0.24	2.71 ± 0.18
45.0	7.08 ± 0.38	2.71 ± 0.23	0.52 ± 0.15	1.16 ± 0.27	3.37 ± 0.19
50.0	7.09 ± 0.42	3.14 ± 0.27	0.67 ± 0.17	1.05 ± 0.29	4.29 ± 0.21
55.0	6.58 ± 0.46	3.87 ± 0.30			
60.0			0.69 ± 0.22	1.41 ± 0.35	5.31 ± 0.26
70.0	4.96 ± 0.48	4.74 ± 0.32	0.69 ± 0.19	0.67 ± 0.29	6.16 ± 0.22
80.0	4.03 ± 0.44	5.24 ± 0.30	0.69 ± 0.24	1.51 ± 0.34	6.12 ± 0.26
90.0	3.74 ± 0.40	4.78 ± 0.27	0.97 ± 0.22	1.75 ± 0.30	5.47 ± 0.23
100.0			0.69 ± 0.19	1.19 ± 0.25	5.60 ± 0.20
105.0	3.30 ± 0.36	5.69 ± 0.24			
120.0			0.53 ± 0.21	1.14 ± 0.24	5.38 ± 0.20
130.0	3.14 ± 0.37	4.75 ± 0.24			
150.0	2.54 ± 0.38	3.87 ± 0.24	0.48 ± 0.21	1.43 ± 0.22	4.56 ± 0.19
200.0	3.26 ± 0.30	2.86 ± 0.19	0.78 ± 0.26	1.85 ± 0.23	4.16 ± 0.21
250.0	3.56 ± 0.32	2.94 ± 0.19	0.55 ± 0.30	1.38 ± 0.23	3.90 ± 0.22
300.0	4.49 ± 0.35	3.60 ± 0.20	0.51 ± 0.35	0.94 ± 0.23	3.71 ± 0.23
350.0	5.08 ± 0.22	3.43 ± 0.12	1.04 ± 0.28	1.36 ± 0.16	3.28 ± 0.18
400.0	5.21 ± 0.31	3.23 ± 0.17	0.58 ± 0.35	0.89 ± 0.18	3.49 ± 0.21
500.0	5.09 ± 0.23	4.52 ± 0.13	1.58 ± 0.38	1.15 ± 0.17	2.73 ± 0.21
600.0	6.07 ± 0.22	4.58 ± 0.12	1.79 ± 0.49	1.81 ± 0.19	2.41 ± 0.24
700.0	6.41 ± 0.24	4.83 ± 0.12	1.74 ± 0.43	1.35 ± 0.15	2.39 ± 0.20
800.0			1.02 ± 0.43	1.65 ± 0.14	2.49 ± 0.19
900.0	6.02 ± 0.28	5.24 ± 0.13	0.79 ± 0.52	1.96 ± 0.15	2.40 ± 0.21
1000.0	6.17 ± 0.33	6.46 ± 0.15	1.90 ± 0.64	2.22 ± 0.18	1.81 ± 0.25
1100.0	5.81 ± 0.50	6.01 ± 0.21	1.47 ± 0.46	2.47 ± 0.12	1.91 ± 0.17
1200.0	5.95 ± 0.39	7.05 ± 0.17	1.21 ± 0.64	2.44 ± 0.17	1.96 ± 0.24
1500.0	6.12 ± 0.39	8.56 ± 0.16	0.37 ± 0.60	2.59 ± 0.16	1.98 ± 0.21

Table 2.

H atom kinetic energy	H(1s)+Xe→H(nl) integral cross sections (10^{-17} cm^2)				
	σ_{2s}	σ_{2p}	σ_{3s}	σ_{3p}	σ_{3d}
10.6		0.02 ± 0.04			
11.5		0.02 ± 0.04			
12.0	0.01 ± 0.05	0.03 ± 0.04			
12.5	0.04 ± 0.05	0.02 ± 0.04			
13.0	0.02 ± 0.05	0.04 ± 0.04			
13.5		0.00 ± 0.05			
14.0	0.10 ± 0.05	0.01 ± 0.04			
15.0	0.14 ± 0.05	0.10 ± 0.04			
16.0	0.08 ± 0.04	0.11 ± 0.05			
17.0	0.30 ± 0.16	0.28 ± 0.14			
18.0	0.32 ± 0.07	0.28 ± 0.06			
20.0	0.36 ± 0.06	0.35 ± 0.05			
22.0	0.57 ± 0.10	0.42 ± 0.07			
25.0	0.52 ± 0.05	0.47 ± 0.05			
30.0	0.72 ± 0.05	0.81 ± 0.06			
35.0	0.83 ± 0.04	1.08 ± 0.05			
40.0	0.89 ± 0.05	1.51 ± 0.07			
45.0	0.90 ± 0.07	1.68 ± 0.12			
50.0	0.94 ± 0.05	2.23 ± 0.09			
60.0	0.67 ± 0.04	2.35 ± 0.09			
70.0	0.57 ± 0.07	2.60 ± 0.04	−0.04 ± 0.04	0.19 ± 0.06	0.21 ± 0.04
80.0	0.39 ± 0.07	2.40 ± 0.04	0.13 ± 0.03	0.38 ± 0.04	0.13 ± 0.03
90.0	0.40 ± 0.06	2.34 ± 0.04	0.09 ± 0.04	0.42 ± 0.06	0.28 ± 0.04
100.0	0.44 ± 0.06	2.27 ± 0.04	0.08 ± 0.05	0.31 ± 0.06	0.39 ± 0.05
120.0	0.60 ± 0.08	2.48 ± 0.05	0.09 ± 0.05	0.44 ± 0.06	0.57 ± 0.05
150.0	0.82 ± 0.09	2.15 ± 0.06	0.28 ± 0.07	0.64 ± 0.07	0.73 ± 0.06
175.0	1.09 ± 0.10	2.04 ± 0.06	0.20 ± 0.07	0.64 ± 0.07	0.95 ± 0.06
200.0	1.15 ± 0.12	1.76 ± 0.07	−0.05 ± 0.10	0.74 ± 0.08	1.23 ± 0.08
225.0			0.18 ± 0.09	0.80 ± 0.07	1.21 ± 0.06
250.0	1.60 ± 0.18	2.24 ± 0.10	0.09 ± 0.08	0.74 ± 0.06	1.41 ± 0.06
270.0			0.00 ± 0.10	0.84 ± 0.07	1.49 ± 0.07
300.0	1.62 ± 0.13	2.12 ± 0.07	0.41 ± 0.10	0.89 ± 0.07	1.37 ± 0.07
320.0			0.16 ± 0.14	0.83 ± 0.09	1.52 ± 0.09
350.0	1.69 ± 0.11	2.47 ± 0.06	0.23 ± 0.11	0.84 ± 0.06	1.45 ± 0.07
400.0	1.63 ± 0.12	2.82 ± 0.07	0.56 ± 0.13	0.98 ± 0.07	1.28 ± 0.08
450.0	1.71 ± 0.13	3.10 ± 0.07	0.30 ± 0.22	1.03 ± 0.11	1.49 ± 0.13
500.0	1.69 ± 0.14	3.29 ± 0.08	0.14 ± 0.14	1.06 ± 0.06	1.51 ± 0.08
550.0			0.32 ± 0.15	1.08 ± 0.06	1.43 ± 0.08
600.0	1.62 ± 0.14	3.93 ± 0.08	0.74 ± 0.23	1.02 ± 0.09	1.31 ± 0.11
700.0	1.45 ± 0.11	4.25 ± 0.06	0.46 ± 0.20	1.39 ± 0.08	1.21 ± 0.10
800.0	1.44 ± 0.14	4.84 ± 0.07	−0.40 ± 0.32	1.36 ± 0.10	1.55 ± 0.14
900.0	1.34 ± 0.16	5.05 ± 0.08	1.24 ± 0.38	1.40 ± 0.12	1.05 ± 0.16
1000.0	1.16 ± 0.16	5.29 ± 0.08	0.71 ± 0.39	1.54 ± 0.11	1.17 ± 0.16
1100.0	1.07 ± 0.20	5.49 ± 0.10	−0.19 ± 0.64	1.96 ± 0.17	1.52 ± 0.24
1200.0	1.07 ± 0.19	5.73 ± 0.09	−0.21 ± 0.73	1.79 ± 0.19	1.51 ± 0.27
1500.0	0.66 ± 0.19	5.77 ± 0.09	0.82 ± 0.73	1.89 ± 0.19	1.18 ± 0.25

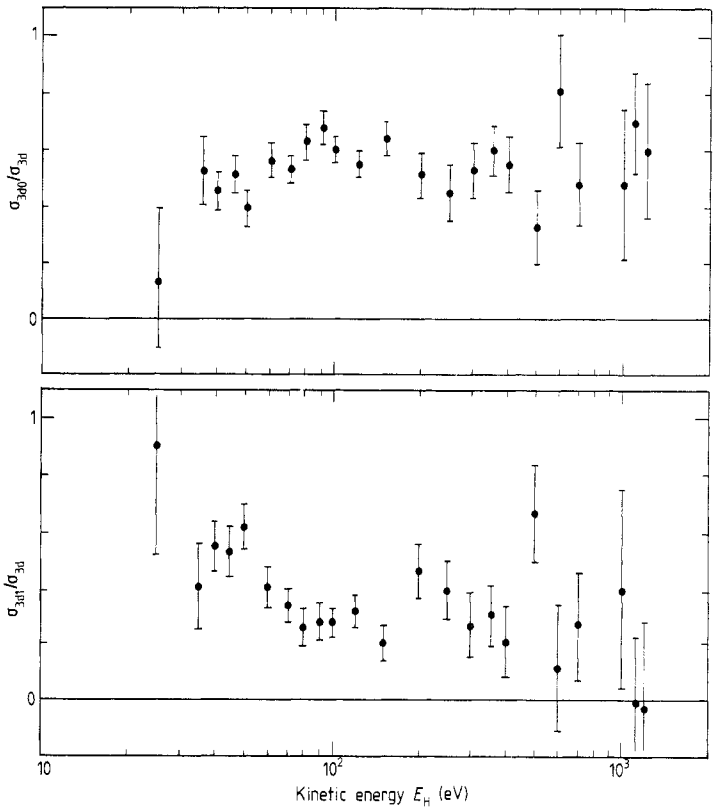

Figure 4. σ_{3d0}/σ_{3d} and σ_{3d1}/σ_{3d} for H + Ar as a function of the collision energy.

by about 10% than the data shown in this case, and the 3p cross section would be reduced by about a factor of two. In order to avoid a systematic error in the H_α-L_α calibration factor, the factor was derived only from Ar data. Finally, data points at energies below 15 eV might be systematically too low, due to the difficulties in monitoring the beam profile (section 2); as the results were always well reproducible, we do not expect this effect to exceed the order of 30%. We summarise as follows.

σ_{2s} is free of systematic errors, except perhaps for the lowest energies.

The quantity labelled σ_{2p} is a weighted sum over the partial cross sections, $\sigma_{2p} = 1.13\sigma_{2p0} + 0.94\sigma_{2p1}$. It is essentially free of systematic errors, again except perhaps for the lowest energies. A small error might be caused by higher cascades, but this is usually negligible and should not exceed 10-20% in the most unfavourable cases.

σ_{3s} is believed to be free of systematic errors. It cannot be excluded with certainty, however, that the additional structure in σ_{3s} for H + Ar at low energy is an artefact caused by a 4f cascade contribution.

σ_{3p} for Ar is essentially correct, but errors from a 4f cascade cannot be completely excluded. σ_{3p} for Xe can, in addition, contain errors due to a Xe emission in the H_α region. As this would result in significantly lower cross section values, the 3p data for Xe have rather the character of an upper limit.

σ_{3d} is believed to be essentially $\sigma_{3d} + \sigma_{4f}$, when there is a 4f excitation at all. In the case of Xe the data might be too large by about 10%, when there is a corresponding Xe excitation.

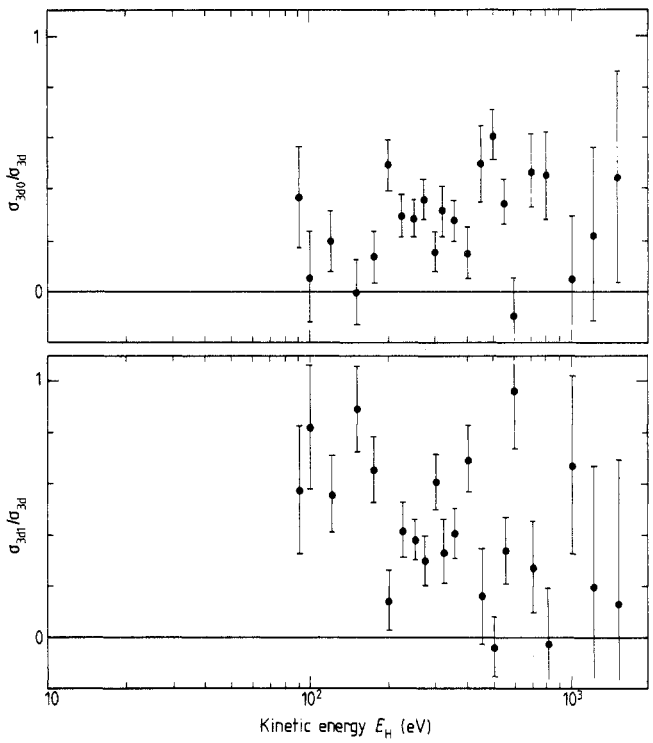

Figure 5. σ_{3d0}/σ_{3d} and σ_{3d1}/σ_{3d} for H+Xe as a function of the collision energy.

The partial cross sections σ_{3dm} are probably very sensitive to cascade effects. A strong 4f contribution to the 3d cross section would make these data rather meaningless. On the other hand, we expect a 4f contribution to result in the first instance in an increase in σ_{3d2}. The smallness of the evaluated σ_{3d2} values might thus indicate the absence of any 4f contribution. There are a number of previous results of other authors with which our data can be compared. Birely and McNeal (1972) measured σ_{2s} and σ_{2p} for energies above 1 keV. The data were not corrected for cascades, the agreement with our data is reasonable, nevertheless. VanZyl and coworkers (VanZyl *et al* 1980, 1986, VanZyl and Gealy 1987) obtained a number of cross section data for the processes in question. Their data for σ_{2p} (1987) are corrected for cascades, but their uncertainty (±15% to ±50%, private communication) is much larger than ours. Taking account of the large uncertainty, the agreement is good, except for H+Ar below 50 eV, where VanZyl's data are too low. VanZyl's data for σ_{3s} (1980, 1986), on the other hand, have a much smaller uncertainty than ours (our 3s data are obtained as a small contribution to a large signal and therefore have a large statistical uncertainty). The agreement is reasonable, once more. We find comparatively large values, however, for σ_{3s} for H+Ar below 200 eV. The VanZyl results do not cover this energy region. The other production cross section data (2s, 3p, 3d and the low-energy results for 2p and 3s) are reported here for the first time. The VanZyl group measured a number of emission cross sections, which can be expressed as linear combinations of the production cross sections σ_{nl}. Such combinations can of course be calculated from our data. With one minor exception (the L_α emission cross section from H+Ar below 50 eV), there is always a perfect agreement between these data sets.

Figures 6 and 7 are collections of the presently known partial collision cross sections for H+Ar and H+Xe. The curves are smooth interpolations through the data points, they are based on the data with the highest accuracy available. These are the present results for σ_{2s}, σ_{2p}, σ_{3p}, and σ_{3d}. σ_{3p} for H+Xe is omitted in view of the possible systematic errors. σ_{3s} for H+Ar is combined from the present data and those of VanZyl *et al* (1980). σ_{3s} for H+Xe as well as the $n=4$ data are from VanZyl *et al* (1980, 1986). The curves labelled H(4p, 4d) show $\sigma_{4d}+0.16\sigma_{4p}$. The charged channels were taken from VanZyl *et al* (1977, H+Ar at higher energy), and Aberle *et al* (1979, 1980, H+Ar at lower energy and H+Xe).

4.2. Off-diagonal terms

Off-diagonal terms are evaluated from the differences $I(F)-I(-F)$ in both the L_α and the H_α signals, as in figure (2*b*). Cascades can contribute to these data as well as to the cross section measurements. The correction of the L_α data for cascades is

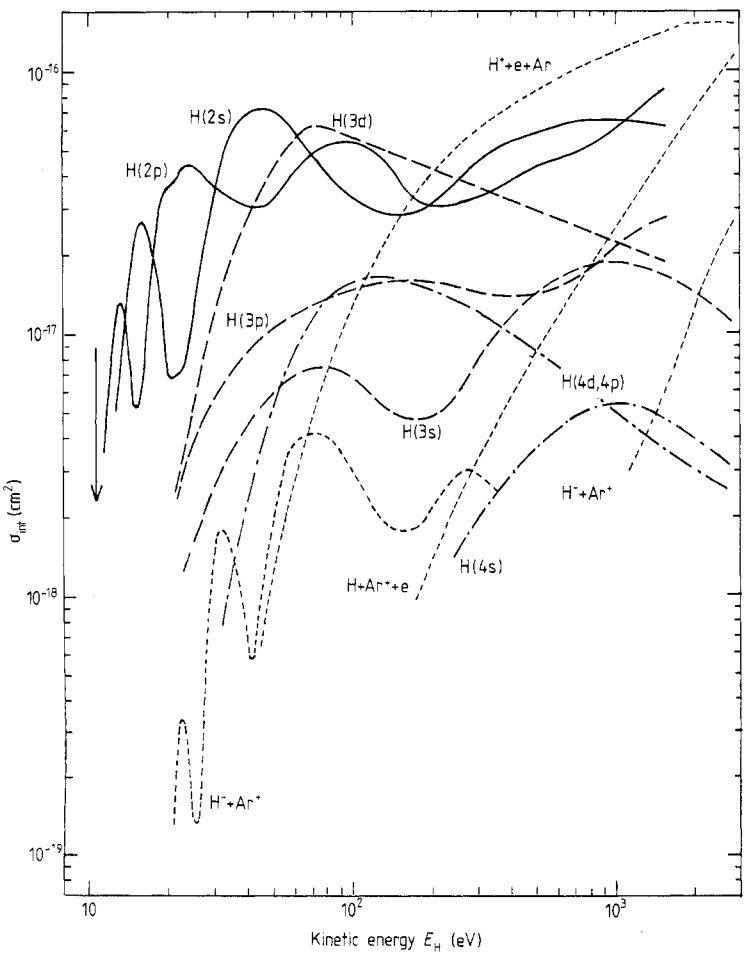

Figure 6. H+Ar: The presently known inelastic cross sections below 2 keV. The arrow indicates the threshold for H($n=2$) production. For the origin of the data, see text.

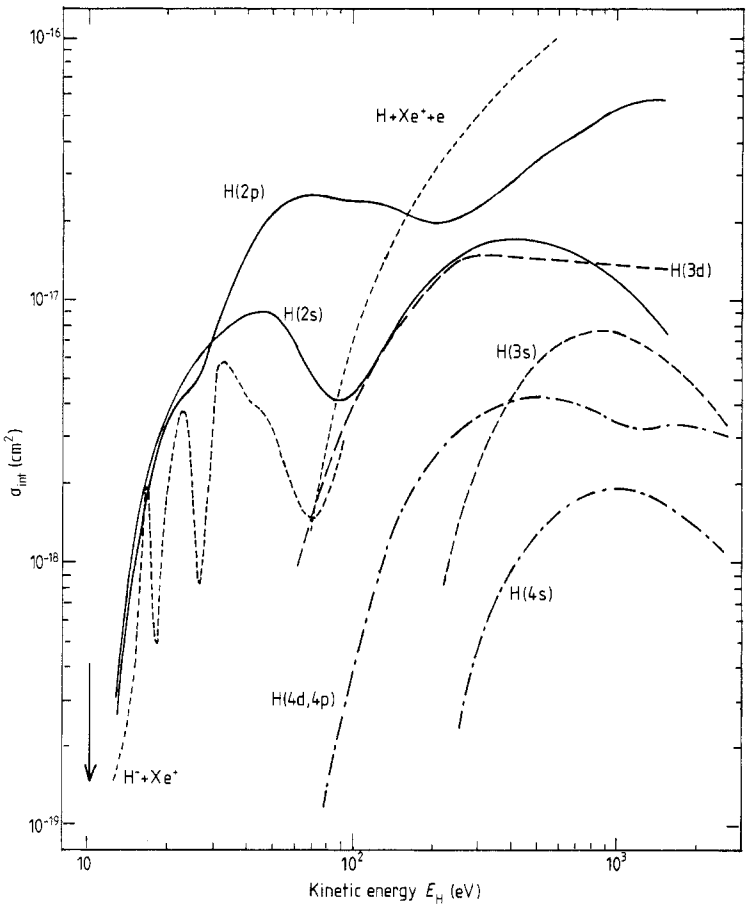

Figure 7. H+Xe: The presently known inelastic cross sections below 2 keV. The arrow indicates the threshold for H($n=2$) production. The present result for σ_{3p} is too uncertain and is omitted. For the origin of the data, see text.

very much simplified by the fact that the pairs of curves $u_{3lm,3l'm}(L_\alpha, F)$ and $u_{3lm,3l'm}(H_\alpha, F)$ for $l \neq l'$ are always very similar. The cascade correction for the L_α differences is therefore carried out by simply subtracting the experimental H_α differences; the relative scaling of the two data sets is known from the procedure described above. The cascade-corrected L_α difference is then fitted to the theoretical curve Re $u_{2s0,2p0}$, giving the sp coherence term Re $\sigma_{2s0,2p0}$. There is an imaginary part as well, but as Im $u_{2s0,2p0}$ is very small, it is not visible in the experimental result. Results for $\sigma_{2s0,2p0}/\sqrt{\sigma_{2s}\sigma_{2p}}$ for H+Ar and H+Xe are shown in figures 8 and 9. Note that

$$\sigma_{nlm,nl'm} \leq \sqrt{\sigma_{nlm}\sigma_{nl'm}}. \tag{7}$$

Our experimental data have a large statistical uncertainty. This has two reasons. First, even the largest possible sp coherence gives rise only to a moderate difference $I(F) - I(-F)$, and second, the quantity which we evaluate is the difference between the H_α and the L_α differences, both of which are themselves small. As demonstrated by figure 2(b), there is often a pronounced difference $I(F) - I(-F)$ in the L_α data for Ar down

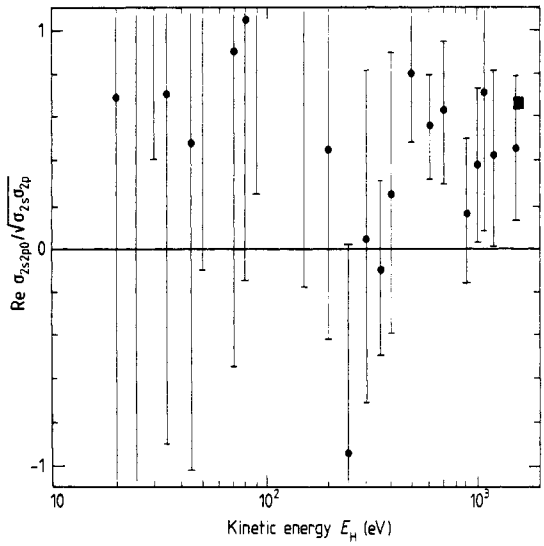

Figure 8. The sp coherence Re $\sigma_{2s,2p0}$ for H+Ar. The square is from Krotkov and Stone (1980).

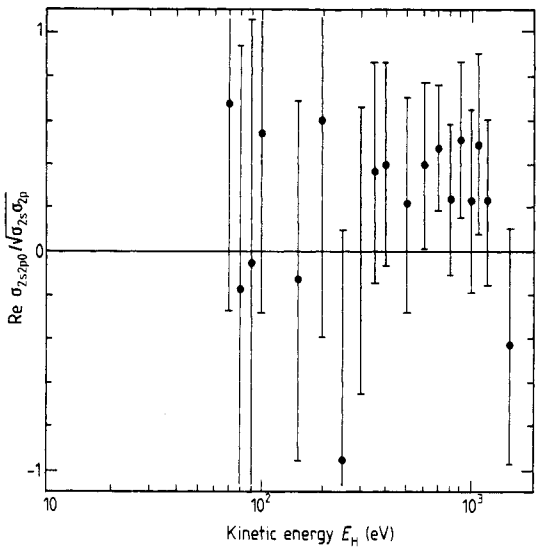

Figure 9. The sp coherence Re $\sigma_{2s,2p0}$ for H+Xe.

to collision energies of about 30 eV. However, as witnessed by the similarity of the H_α and the L_α results in figure 2(*b*), this seems to be mainly a cascade effect. Figure 8 includes a data point obtained by Krotkov and Stone (1980). These authors did not correct for cascades. When we evaluate our L_α data without a cascade correction, we obtain a value very close to that of Krotkov and Stone. Obviously, the missing cascade correction in their work results in an overestimation of $\sigma_{2s,2p0}$.

The evaluation of the $n=3$ off-diagonal terms is less straightforward. Even when higher cascades are disregarded, the experimental result $I(F)-I(-F)$ is the superposition of six different curves $u(F)$ with unknown factors (three terms with independent real and imaginary parts). We performed a trial evaluation, in which only the terms with the largest weighting factors, Re $u_{3p0,3d0}$, Im $u_{3p0,3d0}$, and Re $u_{3p1,3d1}$, are retained. The results are shown in figures 10 and 11. We expect these results to give a reasonable qualitative picture for the following reasons.

(i) Cascades from $n=4$ give a small H_α intensity, as already explained above. This implies that the $n=4$ cascade contribution to the H_α differences is small as well. $n=4$ cascades should rather become visible as cascades in the L_α difference. The nearly perfect cancelling of the H_α and the L_α differences below 500 eV seems to imply that cascades from $n=4$ have no influence at all. (ii) The neglected $n=3$ terms are typically a factor of ten smaller than those retained.

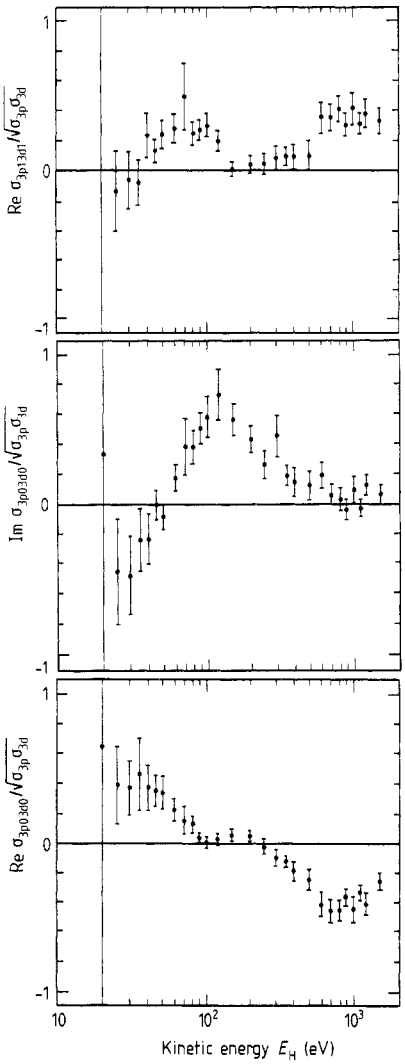

Figure 10. $n=3$ coherence terms for H+Ar.

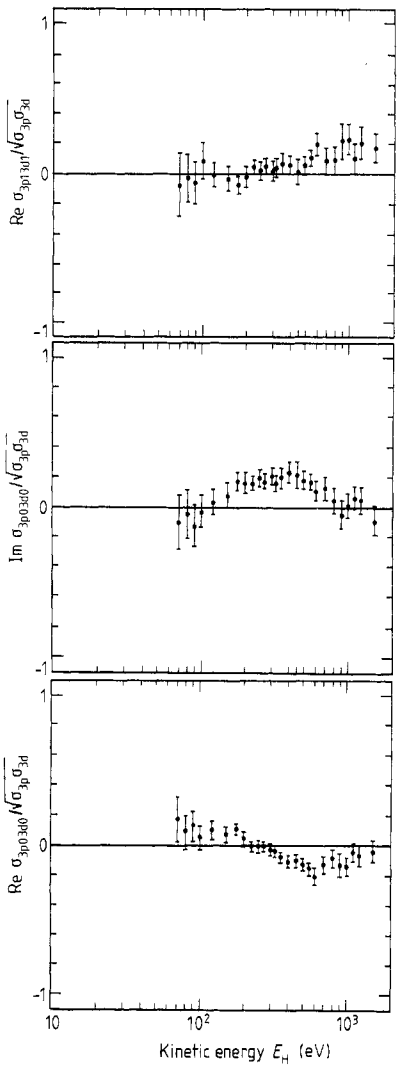

Figure 11. $n=3$ coherence terms for H+Xe.

5. Discussion

It is characteristic for the investigated systems that a multitude of channels is populated even at very low collision energy, and that some cross sections show large amplitude oscillations as a function of the energy. Even when one considers only the channels with the largest cross sections (H(2s, 2p, 3d) for H+Ar), a detailed discussion requires the knowledge of the potentials and the mutual couplings for a significant number of molecular states. For H+Ar, these are at least the Π and Σ states dissociating into H(1s, 2s, 2p, 3d)+Ar. The experimental results in figure 4 show that preferably the 3d0 and 3d1 states are populated. This seems to imply that Π and Σ states, but no Δ states are of importance. The observed strong coherence for $n=3$ implies that the states dissociating to H(3p)+Ar are important, as well. Further there are, at large

atomic distance, a number of states $H+Ar^*$, which have energies between the $H(n=2)+Ar$ and $H(n=3)+Ar$ asymptotes. It must be expected that these states interact with those mentioned above. (No experimental information upon the population of these channels is available.) The inelastic couplings, which are first encountered by the collision pair, are certainly located at small atomic distance (few au), because only in this region the molecular ground state is close enough in energy to the excited states. However, the extrapolated ion-pair potential curve (H^-+Ar^+) intersects near 5 au the group of excited states of interest (VanZyl *et al* 1980), and one must expect strong non-adiabatic couplings in this region, therefore. Though the HAr system has been treated repeatedly by quantum chemists (Matcha and Milleur 1978, Vance and Gallup 1980, Berman and Kaldor 1981, Theodorakopoulos *et al* 1984, Dohmann 1986, and Van Hemert *et al* 1986), only a part of the required information is available. Non-adiabatic interactions are reported only in the two most recent papers, but these are interactions at small distance, only. The excited Ar states were included only by Vance and Gallup. They report marked structures for the potential curves of the third and higher excited Σ states near 5 au, probably indicating non-adiabatic couplings. States dissociating to $H(n=3)+Ar$ were taken into account by Berman and Kaldor, but as the Ar^* states were not considered, the value of these results is questionable. The HXe system, which has similar properties, has not yet been treated quantum chemically. The general lack of information allows no more than a preliminary discussion of the mechanisms, which govern the inelastic collision. Especially, nothing can be said about the origin of the large 3d excitation for H+Ar.

The large amplitude oscillations in some of the channels are a prominent feature of the results in figures 6 and 7. They can be explained as Rosenthal oscillations (Rosenthal and Foley 1969, Ankudinov *et al* 1971). With the Rosenthal mechanism, the sum over all inelastic cross section must be a smooth, non-oscillating function of the energy. In the simplest case, one can expect every channel with an oscillating cross section to be accompanied by a complementary channel, showing opposite phase oscillations of the same amplitude. The complementary oscillations for the ion pair channel for H+Ar might be hidden in any of the larger cross sections. The required amplitude is comparatively small, and the opposite phase oscillations would practically not be visible. For H+Xe, the channel H(2p)+Xe shows some structure which is partly opposite to the oscillations in the ion pair channel, but at the smallest energies, the amplitude is too small. One must conclude that the opposite phase oscillations occur in a channel, which has not yet been investigated, e.g. a $H+Xe^*$ channel. The 2s and 2p channels in H+Ar, finally, show clear opposite phase oscillations, as expected.

The frequency of the Rosenthal oscillations is related to the area between the potential curves, which take part in the Rosenthal mechanism (see Aberle *et al* 1980 for the form of this relation which applies at low collision energies). From the experimental data for the 2s and 2p channels for H+Ar, we deduce a value of 4.4 eV au for this area. We used a numerical program by Peyerimhoff and coworkers to perform CI calculations for the lowest HAr potential curves at distances up to 10 au, where the 2s and 2p curves have converged. The results are in good agreement with the previous data. According to Dohmann (1986), a strong radial coupling between the ground state and the first excited states of HAr occurs near 2 au. The area enclosed between the calculated second and third Σ potential curves between 2 au and 10 au is 2.8 eV au, definitely smaller than the experimental value. There are two possible explanations for the discrepancy. The typical uncertainty of present day quantum chemical data is

estimated to be 0.1 to 0.2 eV (Bruna and Peyerimhoff 1987). An error of this magnitude over the entire range from 2 to 10 au would account for the discrepancy. Also, when other molecular states take part in the Rosenthal mechanism, a larger area is to be expected.

We show finally that the observation of the Rosenthal oscillations allows certain conclusions to be drawn on the nature of the molecular electronic eigenstates. The primary inelastic process in the collision is the double passage through the interaction regions at short distance. This results in the production of a pair of atoms, which are travelling apart, and which are in molecular states $|1\Sigma\rangle$ or $|2\Sigma\rangle$, with amplitudes f_1 or f_2. The amplitudes depend upon the impact parameter and they depend weakly upon the collision energy. When travelling apart, towards infinite distance, there evolves an additional phase difference $\Delta\Phi$ between the two states, which is the origin of the Rosenthal oscillations. $\Delta\Phi$ depends upon the energy but practically not upon the impact parameter. The final state of the system is then

$$f_1|1\Sigma\rangle + f_2|2\Sigma\rangle \exp(i\Delta\Phi). \tag{8}$$

At intermediate and large atomic distance, the molecular states $|1\Sigma\rangle$ and $|2\Sigma\rangle$ leading to the asymptotic states $H(n=2)+Ar$ are linear combinations, essentially

$$\begin{aligned} |1\Sigma\rangle &= c|2s\sigma\rangle + s|2p\sigma\rangle) \\ |2\Sigma\rangle &= -s|2s\sigma\rangle + c|2p\sigma\rangle) \end{aligned} \tag{9}$$

with $c^2+s^2=1$. Insertion of equation (9) into equation (8) gives the amplitudes and hence the diagonal and off-diagonal cross sections for the states 2s and $2p\sigma$:

$$\begin{aligned} |f_{2s}|^2 &= \sigma_1 c^2 + \sigma_2 s^2 - \sigma_{12} 2sc \cos(\Delta\Phi + \Phi_{12}) \\ |f_{2p\sigma}|^2 &= \sigma_1 s^2 + \sigma_2 c^2 + \sigma_{12} 2sc \cos(\Delta\Phi + \Phi_{12}) \\ Ref_{2s} f^*_{2p\sigma} &= (\sigma_1 - \sigma_2)sc + \sigma_{12}(c^2 - s^2)\cos(\Delta\Phi + \Phi_{12}) \end{aligned} \tag{10}$$

with σ_1, σ_2, σ_{12}, and Φ_{12} quantities, which vary slowly with the collision energy. As they stand, the relations apply to the differential cross sections. But when the scattering is essentially forward, equation (10) can be applied, at least in a qualitative sense, to the integral cross sections as well. It is seen that the coefficients c and s can be obtained by comparing the amplitude of the oscillations in the cross sections with that of the corresponding oscillations in the sp coherence term. For instance, for $c=1$ and $s=0$, one can have oscillations in the coherence term, but not in the cross sections, whereas for $s=c=2^{-1/2}$, oscillations can occur in the cross sections, but not in the coherence term. Our measurements of the sp coherence are not good enough to decide, whether σ_{2s2p0} shows marked oscillations or not. But the very fact that we observe oscillations in the cross sections leads to the conclusion that the molecular eigenstates are not of pure 2s and 2p character. Indeed, according to the results of Vance and Gallup (1980), one has roughly $c \simeq s \simeq 2^{-1/2}$.

References

Aberle W, Grosser J and Krüger W 1979 *Chem. Phys.* **41** 245–55

—— 1980 *J. Phys. B: At. Mol. Phys.* **13** 2083–97

Ankudinov V A, Bobahev S V and Perel V I 1971 *Zh. Eksp. Teor. Fiz.* **60** 906–19 (Engl. transl. *Sov. Phys.-JETP* **33** 490–6)

Berman M, Kaldor U 1981 *Chem. Phys.* **63** 165–73

Bevington P R 1969 *Data Reduction and Error Analysis for the Physical Sciences* (New York: McGraw-Hill)
Birely J H and McNeal R J 1972 *Phys. Rev.* A **5** 257-65
Bruna P J and Peyerimhoff S D 1987 *Adv. Chem. Phys.* **67** 1-97
Dohmann H 1986 *Dissertation*, Bonn
Dose V, Gunz R and Meyer V 1968 *Helv. Phys. Acta* **41** 269-73
Fleischmann H H and Young R A 1969 *Phys. Rev.* **178** 254-60
Grisaru M T, Pendleton H N and Petrasso R 1973 *Ann. Phys., NY* **79** 518-41
Grosser J and Krüger W 1985 *Z. Phys.* A **320** 155-6
Knize R J, Lundeen S R and Pipkin F M 1984 *Phys. Rev.* A **29** 1114-30
Krotkov R and Stone J 1980 *Phys. Rev.* A **22** 473-82
Matcha R L and Milleur M B 1978 *J. Chem. Phys.* **69** 3016-24
Orbeli A L, Andreev E P, Ankudinov V A and Dukelskii V M 1969 *Zh. Eksp. Teor. Fiz.* **57** 108 (Engl. transl. 1970 *Sov. Phys.-JETP* **30** 63-7)
Rosenthal H and Foley H M 1969 *Phys. Rev. Lett.* **23** 1480-3
Rouze N, Havener C C, Westerveld W B and Risley J S 1986 *Phys. Rev.* **33** 294-300
Theodorakopoulos G, Stavros C F, Buenker R J and Peyerimhoff S D 1984 *J. Phys. B: At. Mol. Phys.* **17** 1453-62
Vance R L and Gallup G A 1980 *J. Chem. Phys.* **73** 894-901
Van Hemert M C, Dohmann H and Peyerimhoff S D 1986 *Chem. Phys.* **110** 55-66
VanZyl B and Gealy M W 1987 *Phys. Rev.* A **35** 3741-48
VanZyl B, Le T Q, Neumann H and Amme R C 1977 *Phys. Rev.* A **15** 1871-86
VanZyl B, Neumann H and Gealy M W 1986 *Phys. Rev.* A **33** 2093-4
VanZyl B, Neumann H, Rothwell H L Jr and Amme R C 1980 *Phys. Rev.* A **21** 716-29
VanZyl B, VanZyl B K and Westerveld W B 1988 *Phys. Rev.* A **37**, 4201-6